

## An Improved Deadbeat Predictive Current Control with Online Parameter Identification for Surface-Mounted PMSMs

Yao, Yu; Huang, Yunkai; Peng, Fei; Dong, Jianning; Zhang, Hanqi

**DOI**

[10.1109/TIE.2019.2960755](https://doi.org/10.1109/TIE.2019.2960755)

**Publication date**

2020

**Document Version**

Final published version

**Published in**

IEEE Transactions on Industrial Electronics

**Citation (APA)**

Yao, Y., Huang, Y., Peng, F., Dong, J., & Zhang, H. (2020). An Improved Deadbeat Predictive Current Control with Online Parameter Identification for Surface-Mounted PMSMs. *IEEE Transactions on Industrial Electronics*, 67(12), 10145-10155. Article 8941282. <https://doi.org/10.1109/TIE.2019.2960755>

**Important note**

To cite this publication, please use the final published version (if applicable).  
Please check the document version above.

**Copyright**

Other than for strictly personal use, it is not permitted to download, forward or distribute the text or part of it, without the consent of the author(s) and/or copyright holder(s), unless the work is under an open content license such as Creative Commons.

**Takedown policy**

Please contact us and provide details if you believe this document breaches copyrights.  
We will remove access to the work immediately and investigate your claim.




***Green Open Access added to TU Delft Institutional Repository***

***'You share, we take care!' - Taverne project***

**<https://www.openaccess.nl/en/you-share-we-take-care>**

Otherwise as indicated in the copyright section: the publisher is the copyright holder of this work and the author uses the Dutch legislation to make this work public.

# An Improved Deadbeat Predictive Current Control With Online Parameter Identification for Surface-Mounted PMSMs

Yu Yao , Student Member, IEEE, Yunkai Huang , Fei Peng, Member, IEEE, Jianning Dong , Member, IEEE, and Hanqi Zhang

**Abstract**—In this article, an improved deadbeat predictive current control (DPCC) method with parameters identification for surface-mounted permanent magnet synchronous machines (SPMSMs) is proposed. With the proposed DPCC method, zero steady-state current error and deadbeat dynamic current response could be achieved, even with inaccurate initial motor parameters. On basis of the conventional DPCC method, a novel parameters identification for the stator resistance and inductance is developed, which is the main contribution of this article. The proposed parameters identification method works based on a reconstructed characteristic vector from the disturbance observer with current injection. Compared with traditional recursive-least-square methods, the proposed method can be implemented with greatly reduced computation burden. Additionally, since the design is established based on the fully discretized model, the effectiveness will be guaranteed on both low-frequency and high-frequency motors, which is a significant advantage of the proposed method.

**Index Terms**—Deadbeat predictive current control (DPCC), disturbance observer, parameters identification, surface-mounted permanent magnet synchronous machines (SPMSM).

## I. INTRODUCTION

**B**ENEFITING from its advantages of high efficiency, high power density, and excellent control performance, the permanent magnet synchronous machine (PMSM) has been widely used in applications such as robot joints, industrial servo motors, and actuators. Fast and accurate response is usually required for these applications. Therefore, as the most inner control loop of

Manuscript received May 9, 2019; revised September 5, 2019; accepted November 26, 2019. Date of publication December 24, 2019; date of current version August 18, 2020. This work was supported in part by the National Natural Science Foundation of China under Grant 51777034 and Grant 51707037 and in part by the Natural Science Foundation of Jiangsu Province of China under Grant BK20161426. (Corresponding author: Yunkai Huang.)

Y. Yao, Y. Huang, F. Peng, and H. Zhang are with the School of Electrical Engineering, Southeast University, Nanjing 210096, China (e-mail: yuyao@seu.edu.cn; huangyk@seu.edu.cn; pengfei@seu.edu.cn; zhanghanqi@seu.edu.cn).

J. Dong is with the Delft University of Technology, 2628 CD Delft, The Netherlands (e-mail: j.dong-4@tudelft.nl).

Color versions of one or more of the figures in this article are available online at <http://ieeexplore.ieee.org>.

Digital Object Identifier 10.1109/TIE.2019.2960755

the system, the dynamic and steady-state performance of the current control loop is very important for the whole system.

The design of the inner current controller has been extensively researched, various controller methods such as proportional-integral controller [1], [2], state-feedback controller [3], [4], and predictive current control [5]–[8] have been proposed and improved. Among these control methods, the predictive control (PC) method is gaining popularity because of its simple structure and good control performance. According to [9], this kind of control method is classified into two categories: 1) direct PCs and 2) indirect PCs. For the direct PCs, the status of the power switches are controlled directly and no modulator is used. On the contrary, for the indirect PCs, the pulsewidth modulation (PWM) is implemented and the calculated optimal voltage vector can be generated with arbitrary phase and magnitude. Since the PWM is widely used with less current harmonics, this article focuses on the indirect PCs. The indirect PC mainly contains continuous control set model PC (CCS-MPC) and deadbeat predictive current control (DPCC).

The CCS-MPC aims to predict and optimize the voltage command vector to achieve the minimization of the designed cost function at the next sampling period. Small steady-state error and good robustness against the disturbance is achieved. But the effectiveness of the optimization relies on the accuracy of the model parameters. With mismatched parameters, the control performance will be deteriorated. Additionally, the prediction and optimization at every sampling time is computationally heavy, which limits its application. The DPCC method calculates the command voltage based on the discrete-time model [10]. With accurate model parameters, the ideal deadbeat response and zero steady-state error can be achieved at the same time. However, its control performance is extremely sensitive to the model parameters. Because of the errors in the manufacture and assembling progress, there will be mismatch between the real motor parameters and parameters used in the controller. With mismatched parameters adopted in the DPCC, steady-state error and undesirable overshoot may appear. To improve the deteriorated performance resulting from mismatched parameters, the conventional DPCC has been modified in many papers.

In [11], a predictive current control method with current error correction and current-regulated delta modular is proposed. The current error resulting from inaccurate model parameters is reduced, and fast dynamic response is achieved. In [12],

a discrete-time deadbeat direct torque and flux controller for interior PMSMs is developed with stator current and stator flux linkage observer. The effect of the digital delay is eliminated and the deadbeat torque and stator flux linkage control is established. In [13], an improved DPCC method with a unified high-order sliding-mode observer is designed in order to estimate the disturbance in the current loop. The robustness and the tracking accuracy are improved. In [14], an improved DPCC method of the PMSM with sliding-mode stator current and disturbance observer is proposed. The effect of the digital delay is eliminated by the prediction of the stator current. Besides, the robustness and the control accuracy is enhanced by the compensation of the disturbance. In [15], a novel oversampling DPCC method implemented by field-programmable gate array (FPGA) is designed. A disturbance observer is used to achieve high control bandwidth and robustness to parameter variation.

The DPCC methods mentioned above can enhance the control accuracy and the robustness with the mismatched parameters. But they all aim at compensating of the voltage difference caused by the parameters mismatch. Therefore, the ideal DPCC response still could not be achieved. In [16], an improved DPCC method with model reference adaptive system (MRAS) parameter [permanent magnet (PM) flux and stator inductance] identification is proposed. Therefore, the parameter mismatch problem of the PM flux and the stator inductance solved. But the identification of the stator resistance is not considered. In [17], an adaptive robust DPCC method with Luenberger observer and online inductance identification is developed. Besides, multiple parameter identification methods have been investigated by many papers [18]–[21] and most of them are based on recursive least square (RLS) algorithm. The convergence of the estimated parameters in these methods cannot be guaranteed and the heavy matrix computation is also undesirable. Additionally, the proposed method are based on the model approximately discretized by forward Euler method. Therefore, when the operating frequency is adequately high, this method is no more effective.

In order to solve the aforementioned problems, this article proposes an improved DPCC method with parameters identification for surface-mounted permanent magnet synchronous machines (SPMSMs). On basis of the conventional DPCC method consisting of a PC law and a disturbance observer [14], as the main contribution of this article, a novel parameters identification for the stator resistance and inductance is proposed and has the following improvements.

- 1) The proposed parameters identification method works based on a reconstructed characteristic vector from the disturbance observer with current injection. It can be implemented with greatly reduced computation burden compared with the traditional RLS methods.
- 2) The design of the proposed control method is established based on the fully discretized model, which is more accurate than the conventional approximately discretized model. Therefore, the effectiveness will be guaranteed on both low-frequency and high-frequency motors. However, the RLS methods may be difficult to be realized with the fully discretized model.

With the estimated parameters adopted, the parameter mismatch problem is essentially solved and the ideal deadbeat response is achieved. Finally, the effectiveness of the proposed DPCC method is validated by the simulation and experimental results on a 133.3 Hz motor and a 1.33 kHz motor with 10 kHz sampling frequency.

## II. SPMSM MODEL

In this section, the discrete-time model of the SPMSM is developed in the  $\alpha\beta$  stationary frame and the  $dq$  synchronous frame. The continuous-time state-space model of the SPMSM

$$\frac{d}{dt} \mathbf{i}_{\alpha\beta}(t) = \mathbf{A} \mathbf{i}_{\alpha\beta}(t) + \mathbf{B} (\mathbf{v}_{\alpha\beta}(t) - \mathbf{e}_{\alpha\beta}(t)) \quad (1)$$

and

$$\begin{aligned} \mathbf{e}_{\alpha\beta}(t) &= \omega \Psi [-\sin \theta_e \cos \theta_e]^T \\ \frac{d}{dt} \mathbf{e}_{\alpha\beta}(t) &= \omega \mathbf{J} \mathbf{e}_{\alpha\beta}(t) \end{aligned} \quad (2)$$

with

$$\mathbf{A} = \begin{bmatrix} -\frac{R}{L} & 0 \\ 0 & -\frac{R}{L} \end{bmatrix} \mathbf{B} = \begin{bmatrix} \frac{1}{L} & 0 \\ 0 & \frac{1}{L} \end{bmatrix} \mathbf{J} = \begin{bmatrix} 0 & -1 \\ 1 & 0 \end{bmatrix}$$

where  $R$  is the winding resistance and  $L$  is the stator inductance.  $\mathbf{i}_{\alpha\beta} = [i_\alpha \ i_\beta]^T$  the stator current,  $\mathbf{v}_{\alpha\beta} = [v_\alpha \ v_\beta]^T$  the VSI output voltage;  $\mathbf{e}_{\alpha\beta} = [e_\alpha \ e_\beta]^T$  the back electromotive force (EMF);  $\omega$  the rotor electric angular speed;  $\theta_e$  the electrical rotor position; and  $\Psi$  the flux linkage from the permanent magnet.

According to [22], the extended state-space model with (1) and (2) augmented is derived as

$$\frac{d}{dt} \begin{bmatrix} \mathbf{i}_{\alpha\beta}(t) \\ \mathbf{e}_{\alpha\beta}(t) \end{bmatrix} = \begin{bmatrix} \mathbf{A} & -\mathbf{B} \\ 0 & \omega \mathbf{J} \end{bmatrix} \begin{bmatrix} \mathbf{i}_{\alpha\beta}(t) \\ \mathbf{e}_{\alpha\beta}(t) \end{bmatrix} + \begin{bmatrix} \mathbf{B} \\ 0 \end{bmatrix} \mathbf{v}_{\alpha\beta}(t) \quad (3)$$

and the fully discretized form of (3) derived using the zero-order hold method can be expressed as

$$\begin{bmatrix} \mathbf{i}_{\alpha\beta}(k+1) \\ \mathbf{e}_{\alpha\beta}(k+1) \end{bmatrix} = \begin{bmatrix} \mathbf{G}_1 & \mathbf{G}_2 \\ 0 & \mathbf{G}_3 \end{bmatrix} \begin{bmatrix} \mathbf{i}_{\alpha\beta}(k) \\ \mathbf{e}_{\alpha\beta}(k) \end{bmatrix} + \begin{bmatrix} \mathbf{H}_1 \\ 0 \end{bmatrix} \mathbf{v}_{\alpha\beta}(k) \quad (4)$$

with

$$\begin{aligned} \mathbf{G}_1 &= x \mathbf{I} \quad \mathbf{H}_1 = y \mathbf{I} \\ \mathbf{G}_3 &= \begin{bmatrix} \cos(\omega T) & -\sin(\omega T) \\ \sin(\omega T) & \cos(\omega T) \end{bmatrix} \quad \mathbf{G}_2 = \begin{bmatrix} d_1 & -d_2 \\ d_2 & d_1 \end{bmatrix} \end{aligned} \quad (5)$$

$$\begin{aligned} x &= e^{-\frac{R}{L}T} \quad y = \frac{1 - e^{-\frac{R}{L}T}}{R} \\ d_1 &= \frac{(x - \cos(\omega T))R - \sin(\omega T)\omega L}{R^2 + \omega^2 L^2} \\ d_2 &= -\frac{(x - \cos(\omega T))\omega L + \sin(\omega T)R}{R^2 + \omega^2 L^2} \end{aligned} \quad (6)$$

where  $T$  is the sampling period and  $\mathbf{I}$  is the unit matrix.

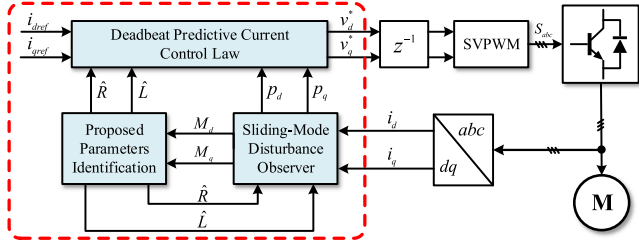


Fig. 1. Proposed DPCC structure with a sliding-mode disturbance observer and parameters identification.

To obtain the discrete-time model in the rotor synchronous  $dq$  reference frame, using coordinate transformation, the discrete-time model in the  $dq$  reference frame is derived as

$$\mathbf{i}_{dq}(k+1) = \mathbf{G}\mathbf{i}_{dq}(k) + \mathbf{H}\mathbf{v}_{dq}(k) + \mathbf{F}\mathbf{e}_{dq}(k) \quad (7)$$

where  $\mathbf{i}_{dq} = [i_d \ i_q]^T$ ,  $\mathbf{v}_{dq} = [v_d \ v_q]^T$ ,  $\mathbf{e}_{dq} = [0 \ \omega\Psi]^T$  and

$$\mathbf{G} = \mathbf{T}_r \mathbf{G}_1 \mathbf{H} = \mathbf{T}_r \mathbf{H}_1 \mathbf{F} = \mathbf{T}_r \mathbf{G}_2$$

$$\mathbf{T}_r = \begin{bmatrix} \cos(\omega(k)T) & \sin(\omega(k)T) \\ -\sin(\omega(k)T) & \cos(\omega(k)T) \end{bmatrix}.$$

### III. PROPOSED DPCC METHOD

In this section, a novel DPCC method is proposed. The proposed DPCC structure is shown in Fig. 1, which consists of the DPCC law, a sliding-mode disturbance observer, and the parameter identification part. Especially, the parameters ( $R$  and  $L$ ) identification part will be executed only when the driven motor is on the steady state, which indicates that  $\omega$  and  $i_q$  stay unchanged. After the estimation of  $R$  and  $L$  converges, this part will be bypassed until the next execution starts.

#### A. DPCC Law

Based on (7), the discrete-time model with the mismatched parameters adopted is derived as

$$\mathbf{i}_{dq}(k+1) = \hat{\mathbf{G}}\mathbf{i}_{dq}(k) + \hat{\mathbf{H}}\mathbf{v}_{dq}(k) + \underbrace{(\mathbf{G} - \hat{\mathbf{G}})\mathbf{i}_{dq}(k) + (\mathbf{H} - \hat{\mathbf{H}})\mathbf{v}_{dq}(k) + \mathbf{F}\mathbf{e}_{dq}(k)}_{\mathbf{p}(k)=[p_d(k) \ p_q(k)]^T} \quad (8)$$

where  $\hat{\mathbf{G}}$  and  $\hat{\mathbf{H}}$  are matrices with the estimated stator resistance and inductance. These matrices are not related with the PM flux linkage.

In addition, the mechanism of the PWM implementation is shown in Fig. 2 and the one-sampling-period delay in the fully digital controller is modeled as

$$\mathbf{v}_{dq}(k+1) = \mathbf{T}_r \mathbf{v}_{dq\_ref}(k) = \mathbf{v}_{dq}^*(k) \quad (9)$$

where  $\mathbf{v}_{dq\_ref}$  is the reference voltage vector and  $\mathbf{v}_{dq}$  is the VSI output voltage.  $\mathbf{v}_{dq}^*(k)$  is defined aiming at marking briefly. In order to compensate the digital delay, (8) should be modified based on the  $k+1$  step and  $k+2$  step and there is

$$\mathbf{i}_{dq}(k+2) = \hat{\mathbf{G}}\mathbf{i}_{dq}(k+1) + \hat{\mathbf{H}}\mathbf{v}_{dq}^*(k) + \mathbf{p}(k+1). \quad (10)$$

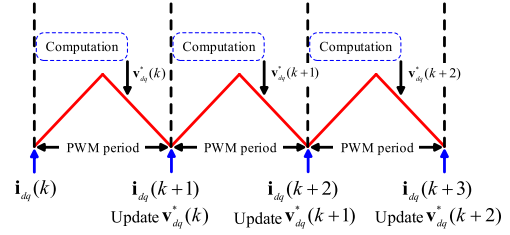


Fig. 2. Mechanism of the PWM implementation.

Normally, the current reference  $\mathbf{i}_{dqref}(k+2)$  is known in advance and the ideal deadbeat current control law could be obtained as

$$\mathbf{v}_{dq}^*(k) = \hat{\mathbf{H}}^{-1}(\mathbf{i}_{dqref}(k+2) - \hat{\mathbf{G}}\mathbf{i}_{dq}(k+1) - \mathbf{p}(k+1)). \quad (11)$$

This control law consists of the predictive current  $\mathbf{i}_{dq}(k+1)$ , which could not be obtained directly. In [14], a predictive current item  $\hat{\mathbf{i}}_{dq}(k+1)$  from a disturbance observer is used to replace  $\mathbf{i}_{dq}(k+1)$ . However, in this article,  $\mathbf{i}_{dqref}(k+1)$  is adopted in the control law instead of  $\mathbf{i}_{dq}(k+1)$ . Besides, a disturbance observer is designed to estimate  $\mathbf{p}(k)$ . Considering the estimated disturbance at  $k+1$  step cannot be obtained directly, therefore the predictive current control law is modified as follows:

$$\mathbf{v}_{dq}^*(k) = \hat{\mathbf{H}}^{-1}(\mathbf{i}_{dqref}(k+2) - \hat{\mathbf{G}}\mathbf{i}_{dqref}(k+1) - \hat{\mathbf{p}}(k)) \quad (12)$$

where  $\hat{\mathbf{p}}(k)$  is the estimated disturbance of  $\mathbf{p}(k)$ , which can be obtained by the disturbance observer. The disturbance observer will be introduced in next section.

#### B. Sliding-Mode Disturbance Observer

A discrete-time sliding-mode observer is designed to estimate the disturbance caused by the parameters perturbation and the back EMF. Based on (8), the sliding-mode disturbance is developed as

$$\hat{\mathbf{i}}_{dq}(k+1) = \hat{\mathbf{G}}\hat{\mathbf{i}}_{dq}(k) + \hat{\mathbf{H}}\mathbf{v}_{dq}(k) + \hat{\mathbf{p}}(k) \quad (13)$$

where  $\hat{\mathbf{i}}_{dq}$  and  $\hat{\mathbf{p}}$  are the estimated current and disturbance, respectively. The error-dynamic equation can be obtained by (8)–(13) and there is

$$\tilde{\mathbf{i}}_{dq}(k+1) = \hat{\mathbf{G}}\tilde{\mathbf{i}}_{dq}(k) + \hat{\mathbf{p}}(k) - \mathbf{p}(k) \quad (14)$$

where  $\tilde{\mathbf{i}}_{dq}(k) = \hat{\mathbf{i}}_{dq}(k) - \mathbf{i}_{dq}(k)$ .

The switching function is defined as

$$\mathbf{s}(k) = [s_d(k) \ s_q(k)]^T = \mathbf{C}\tilde{\mathbf{i}}_{dq}(k) \quad (15)$$

where  $\mathbf{C} \in \mathbf{R}^{2 \times 2}$  is a diagonal matrix with arbitrary eigenvalues. Since the design of the sliding-mode disturbance observer is not the main concern, a nonswitching reaching law is implemented as

$$\mathbf{s}(k+1) = \mathbf{Q}\mathbf{s}(k) + \mathbf{C}(\mathbf{p}(k) - \mathbf{p}(k-1)) \quad (16)$$

where  $\mathbf{Q} \in \mathbf{R}^{2 \times 2}$  is a diagonal matrix with both eigenvalues inside the unit circle.  $\lambda$  denotes the switching gain and is positive. Combing (14), (15), and (16), the attraction function of the

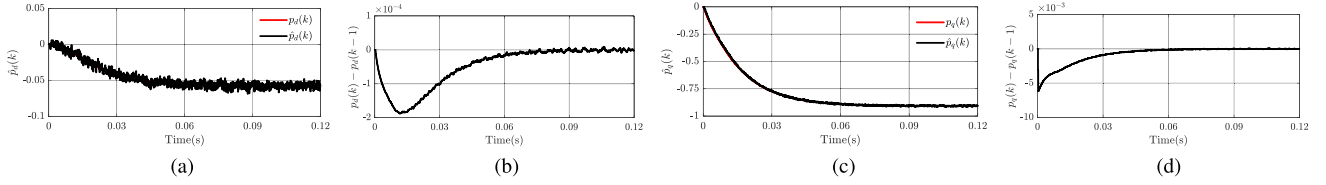


**Fig. 3.**  $\mathbf{p}(k)$  and  $\mathbf{p}(k) - \hat{\mathbf{p}}(k)$  with accurate parameters ( $R$  and  $L$ ) when a motor (see Table I) accelerates up to 133.3 Hz. (a)  $p_d(k)$  and  $\hat{p}_d(k)$ . (b)  $p_d(k) - \hat{p}_d(k)$ . (c)  $p_q(k)$  and  $\hat{p}_q(k)$ . (d)  $p_q(k) - \hat{p}_q(k)$ .

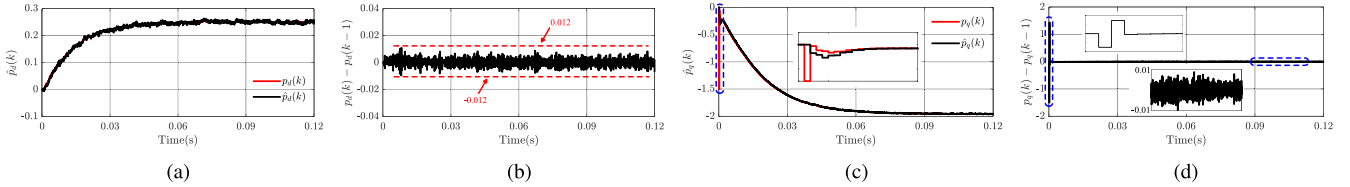


**Fig. 4.**  $\mathbf{p}(k)$  and  $\mathbf{p}(k) - \hat{\mathbf{p}}(k)$  with inaccurate parameters ( $0.5R$  and  $0.5L$ ) when a motor (see Table I) accelerates up to 133.3 Hz. (a)  $p_d(k)$  and  $\hat{p}_d(k)$ . (b)  $p_d(k) - \hat{p}_d(k)$ . (c)  $p_q(k)$  and  $\hat{p}_q(k)$ . (d)  $p_q(k) - \hat{p}_q(k)$ .

**TABLE I**  
PARAMETERS OF THE TESTED LOW-FREQUENCY MOTOR

Symbol	Parameter	Value
$R$	resistance	2.2 $\Omega$
$L_s$	inductance	5.5 mH
$U_{DC}$	DC bus voltage	300 V
$poles$	poles	8
$n_N$	the rated frequency	133.3 Hz

sliding-mode observer is

$$\hat{\mathbf{p}}(k) = \mathbf{C}^{-1} \mathbf{Q} \mathbf{s}(k) - \hat{\mathbf{G}} \tilde{\mathbf{i}}_{dq}(k) + \mathbf{p}(k-1) \quad (17)$$

and based on (14),  $\mathbf{p}(k-1)$  is obtained by

$$\mathbf{p}(k-1) = \hat{\mathbf{G}} \tilde{\mathbf{i}}_{dq}(k-1) + \hat{\mathbf{p}}(k-1) - \tilde{\mathbf{i}}_{dq}(k) \quad (18)$$

Additionally, for the closed-loop system formed by the error dynamic (14) and the attraction function (17), the state of the switching function can be obtained by solving the difference equation (16) as

$$\begin{aligned} \mathbf{s}(k+1) &= \mathbf{Q}^k \mathbf{s}(1) \\ &+ \sum_{j=0}^{k-1} \mathbf{Q}^j \mathbf{C} (\mathbf{p}(k-j-1) - \hat{\mathbf{p}}(k-j)) \end{aligned} \quad (19)$$

where  $\mathbf{s}(1) = \mathbf{Q} \mathbf{s}(0)$ . Because the eigenvalues of the matrix  $\mathbf{Q}$  are inside the unit circle, the item  $\mathbf{Q}^k$  tends to zero matrix, which indicates  $\mathbf{Q}^k \mathbf{s}(1)$  has to converge to zero vector. Therefore, the convergence of the  $\mathbf{s}(k)$  depends on the performance of the  $\mathbf{p}(k-1) - \hat{\mathbf{p}}(k)$ .

Figs. 3 and 4 show the performance of  $\mathbf{p}(k)$ ,  $\hat{\mathbf{p}}(k)$ , and  $\mathbf{p}(k) - \hat{\mathbf{p}}(k)$  when a motor accelerates up to 133.3 Hz. The parameters of the tested motor are listed in Table I. As shown in Fig. 3, when the accurate parameters ( $R$  and  $L$ ) are adopted, the  $\mathbf{p}(k-1) - \hat{\mathbf{p}}(k)$  is adequately small and tends to zero. Based on (19), the  $\mathbf{s}(k)$  will stay within a negligible band and finally

converge to zero. In that case, the  $\mathbf{p}(k)$  can be well estimated by the  $\hat{\mathbf{p}}(k)$ .

Besides, the parameter mismatch is also considered. It is worth noting that  $\hat{\mathbf{G}}$  and  $\hat{\mathbf{H}}$  are matrices with the estimated  $R$  and  $L$ , which is unrelated with the  $\Psi$ . It indicates that the PM flux linkage  $\Psi$  is not used in the proposed method and the parameter mismatch possibly occurs on  $R$  and  $L$ . In Fig. 4, with the inaccurate parameters ( $0.5R$  and  $0.5L$ ) adopted, the  $\mathbf{p}(k)$  is also well estimated by the  $\hat{\mathbf{p}}(k)$ . Therefore, the sliding-mode observer works well to estimate the  $\mathbf{p}(k)$  even with the inaccurate parameters.

### C. Performance Analysis of the Proposed Method

**1) With Accurate Parameters:** When the accurate  $R$  and  $L$  are adopted, as shown in Fig. 3, the  $\mathbf{p}(k) = \mathbf{F} \mathbf{e}_{dq}(k)$  is closely related with the back EMF and varies slowly. Therefore, it can be well estimated by the  $\hat{\mathbf{p}}(k)$ . Besides,  $\mathbf{i}_{dq}(k+1) = \mathbf{i}_{dqref}(k+1)$  holds. Therefore, the ideal deadbeat response of the current tracking system is achieved.

**2) With Inaccurate Parameters:** When the adopted  $R$  and  $L$  are inaccurate, in Fig. 4, the  $p_q(k)$  varies quickly at the beginning because of the mismatched parameters. The  $\hat{p}_q(k)$  gradually converges to  $p_q(k)$ , which indicates the ideal deadbeat current response cannot be achieved.

Substituting (9) and (12) into (10), the dynamic response of the current tracking system can be obtained as

$$\begin{aligned} \mathbf{i}_{dq}(k+2) &= \hat{\mathbf{G}} \mathbf{i}_{dq}(k+1) + \mathbf{i}_{dqref}(k+2) \\ &- \hat{\mathbf{G}} \mathbf{i}_{dqref}(k+1) - \hat{\mathbf{p}}(k) + \mathbf{p}(k+1) \end{aligned} \quad (20)$$

and by solving this equation, there is

$$\begin{aligned} \mathbf{e}_{idq}(k+1) &= \hat{\mathbf{G}}^k \mathbf{e}_{idq}(1) \\ &+ \sum_{j=0}^{k-1} \hat{\mathbf{G}}^j (\mathbf{p}(k-j) - \hat{\mathbf{p}}(k-j-1)) \end{aligned} \quad (21)$$



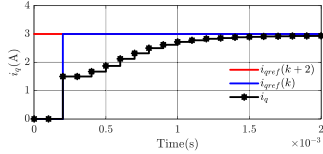


Fig. 5.  $i_q$  and  $i_{qref}$  with inaccurate parameters ( $0.5R$  and  $0.5L$ ).

where  $e_{idq} = \mathbf{i}_{dq} - \mathbf{i}_{dqref}$  denotes the current tracking error vector. Additionally, all the elements of  $\hat{\mathbf{G}}$  is less than 1 and, thus,  $\hat{\mathbf{G}}^k$  tends to a zero matrix. So the control performance of the proposed method depends on the  $\mathbf{p}(k+1) - \hat{\mathbf{p}}(k)$ . As the analysis mentioned above, the  $\mathbf{p}(k+1) - \mathbf{p}(k)$  varies slowly and converges to zero. Besides, because of the disturbance observer, the  $\mathbf{p}(k)$  will be well estimated by the  $\hat{\mathbf{p}}(k)$ . In that case, the  $\mathbf{p}(k+1) - \hat{\mathbf{p}}(k)$  is also gradually decreasing and tends to zero vector. Therefore, the current tracking error will converge to zero. As shown in Fig. 5, because of the mismatched parameters, the ideal deadbeat response cannot be achieved. But with the help of the sliding-mode disturbance observer, the voltage drop caused by the mismatched parameters is well compensated and the static tracking error is eliminated.

#### IV. PARAMETERS IDENTIFICATION METHOD

The DCPD method with the disturbance observer helps eliminate the steady-state error [14]. But the dynamic tracking response is still deteriorated by the parameter mismatch. In order to solve this problem, parameter identification is necessary to achieve the ideal deadbeat response. In this section, a novel parameters identification method is proposed for  $R$  and  $L$ . Since the  $\Psi$  is not used in the proposed method, there is no need to estimate it.

##### A. Reconstructed Characteristic Vector

The proposed parameter identification is based on the characteristic of a reconstructed vector, which is defined as

$$\begin{aligned} \mathbf{M}(k) &= \hat{\mathbf{F}}^{-1} \mathbf{p}(k) \\ &= -\hat{\mathbf{G}}_2^{-1} \tilde{\mathbf{G}}_1 \mathbf{i}_{dq}(k) - \hat{\mathbf{G}}_2^{-1} \tilde{\mathbf{H}}_1 \mathbf{v}_{dq}(k) \\ &\quad + \hat{\mathbf{G}}_2^{-1} \hat{\mathbf{G}}_2 \mathbf{e}_{dq}(k) \end{aligned} \quad (22)$$

where  $\mathbf{M} = [M_d \ M_q]^T$ ,  $\hat{\mathbf{F}} = \mathbf{T}_{k \rightarrow k+1} \hat{\mathbf{G}}_2$  and

$$\begin{aligned} \tilde{\mathbf{G}}_1 &= \hat{\mathbf{G}}_1 - \mathbf{G}_1 \\ \tilde{\mathbf{H}}_1 &= \hat{\mathbf{H}}_1 - \mathbf{H}_1. \end{aligned} \quad (23)$$

The proposed identification method for the  $R$  and  $L$  is based on the variation of the  $\mathbf{M}(k)$  when a negative current is injected into the  $d$ -axis. So before the injection, at time  $t_0$ , the reconstructed vector  $\mathbf{M}(k)$  can be expressed as

$$\begin{aligned} \mathbf{M}(t_0) &= -\hat{\mathbf{G}}_2^{-1} \tilde{\mathbf{G}}_1 \mathbf{i}_{dq}(t_0) - \hat{\mathbf{G}}_2^{-1} \tilde{\mathbf{H}}_1 \mathbf{v}_{dq}(t_0) \\ &\quad + \hat{\mathbf{G}}_2^{-1} \hat{\mathbf{G}}_2 \mathbf{e}_{dq}(t_0). \end{aligned} \quad (24)$$

Then, a negative stepping current is injected into the  $d$ -axis. After the control system reaches the steady state again at time

$t_1$ , it can be obtained that

$$\begin{aligned} \mathbf{M}(t_1) &= -\hat{\mathbf{G}}_2^{-1} \tilde{\mathbf{G}}_1 \mathbf{i}_{dq}(t_1) - \hat{\mathbf{G}}_2^{-1} \tilde{\mathbf{H}}_1 \mathbf{v}_{dq}(t_1) \\ &\quad + \hat{\mathbf{G}}_2^{-1} \hat{\mathbf{G}}_2 \mathbf{e}_{dq}(t_1). \end{aligned} \quad (25)$$

By (24) and (25), the variation of  $\mathbf{M}(k)$  can be derived as

$$\Delta \mathbf{M} = -\hat{\mathbf{G}}_2^{-1} \tilde{\mathbf{G}}_1 \Delta \mathbf{i}_{dq} - \hat{\mathbf{G}}_2^{-1} \tilde{\mathbf{H}}_1 \Delta \mathbf{v}_{dq} \quad (26)$$

where  $\Delta$  refers to the variation between  $t_1$  and  $t_0$ . Unfolding the equations above, there are

$$\Delta M_d(k) = \frac{\Delta W_d}{\hat{d}_1^2 + \hat{d}_2^2} \Delta M_q(k) = \frac{\Delta W_q}{\hat{d}_1^2 + \hat{d}_2^2} \quad (27)$$

with

$$\begin{aligned} \Delta W_d &= -\hat{d}_1(\tilde{x} \Delta i_d + \tilde{y} \Delta v_d) - \hat{d}_2 \tilde{y} \Delta v_q \\ \Delta W_q &= \hat{d}_2(\tilde{x} \Delta i_d + \tilde{y} \Delta v_d) - \hat{d}_1 \tilde{y} \Delta v_q \end{aligned} \quad (28)$$

where  $\tilde{x} = \hat{x} - x$ ,  $\tilde{y} = \hat{y} - y$ ,  $x = e^{-\frac{\hat{R}}{L}T}$ , and  $\hat{y} = \frac{1-e^{-\frac{\hat{R}}{L}T}}{\hat{R}}$ .  $\hat{R}$  and  $\hat{L}$  are the estimated values of  $R$  and  $L$  used in the model, respectively.

Additionally, on basis of (7), the voltage difference between  $t_1$  and  $t_0$  can be obtained as

$$\begin{aligned} \Delta v_d &= \frac{1}{y} (\cos(\omega T) - x) \Delta i_d \\ \Delta v_q &= \frac{1}{y} \sin(\omega T) \Delta i_d. \end{aligned} \quad (29)$$

Based on (28),  $\tilde{x}$  and  $\tilde{y}$  could be directly solved. However, the noise in the estimation of  $\hat{p}(k)$  will bring errors to the results. In this article, a simplified method for the parameter identification is proposed for the low-frequency motor and high-frequency motor, which are defined as follows.

*Definition 1:* An SPMSM is called a low-frequency motor if the winding resistance  $R$ , the stator inductance  $L$ , the electric angular speed  $\omega$ , and the sampling period  $T$  of an SPMSM satisfies

$$\begin{aligned} \cos(\omega T) &\geq 0.98 \\ |e^{-\frac{R}{L}T} - (1 - \frac{R}{L}T)| &< 0.05. \end{aligned} \quad (30)$$

*Definition 2:* An SPMSM is called high-frequency motor if the winding resistance  $R$ , the stator inductance  $L$ , the electric angular speed  $\omega$ , and the sampling period  $T$  of an SPMSM satisfies

$$\begin{aligned} \cos(\omega T) &< 0.98 \\ R &< 0.2\omega L. \end{aligned} \quad (31)$$

##### B. Low-Frequency Motor

With the definition of the low-frequency motor, some equations can be simplified as

- 1)  $\cos(\omega T) \approx 1$  and  $\sin(\omega T) \approx \omega T$ ;
- 2)  $x \approx 1 - \frac{R}{L}T$ ,  $\hat{x} \approx 1 - \frac{\hat{R}}{L}T$ ,  $y \approx \frac{T}{L}$  and  $\hat{y} \approx \frac{T}{L}$ .

Therefore, there are

$$\begin{aligned} \hat{d}_1 &= \frac{(\hat{x} - \cos(\omega T))\hat{R} - \sin(\omega T)\omega\hat{L}}{\hat{R}^2 + \omega^2\hat{L}^2} \\ &\approx \frac{(\hat{x} - 1)\hat{R} - \omega T\omega\hat{L}}{\hat{R}^2 + \omega^2\hat{L}^2} \\ \hat{d}_2 &= -\frac{(\hat{x} - \cos(\omega T))\omega\hat{L} + \sin(\omega T)\hat{R}}{\hat{R}^2 + \omega^2\hat{L}^2} \\ &\approx -\frac{(\hat{x} - 1)\omega\hat{L} + \omega T\hat{R}}{\hat{R}^2 + \omega^2\hat{L}^2} = 0 \end{aligned} \quad (32)$$

$$\begin{aligned} \Delta v_d &= \frac{(1-x)}{y}\Delta i_d = R\Delta i_d \\ \Delta v_q &= \frac{\omega T}{y}\Delta i_d = \omega L\Delta i_d \end{aligned} \quad (33)$$

$$\tilde{x} = \hat{x} - x = \left(\frac{R}{L} - \frac{\hat{R}}{\hat{L}}\right)T\tilde{y} = \hat{y} - y = \frac{L - \hat{L}}{L\hat{L}}T. \quad (34)$$

Substituting (32), (33), and (34) into (28), it can be derived as

$$\begin{aligned} \Delta W_d &= -\hat{d}_1(\tilde{x}\Delta i_d + \tilde{y}\Delta v_d) \\ &= \frac{\hat{R}^2 T + \omega T\omega\hat{L}}{\hat{R}^2 + \omega^2\hat{L}^2} \left[ \left(\frac{R}{L} - \frac{\hat{R}}{\hat{L}}\right) + \frac{L - \hat{L}}{L\hat{L}}R \right] T\Delta i_d \\ &= \frac{\hat{R}^2 T + \omega T\omega\hat{L}}{\hat{R}^2 + \omega^2\hat{L}^2} \frac{T}{\hat{L}}(R - \hat{R})\Delta i_d \end{aligned} \quad (35)$$

and

$$\begin{aligned} \Delta W_q &= -\hat{d}_1\tilde{y}\Delta v_q \\ &= \frac{\hat{R}^2 T + \omega T\omega\hat{L}}{\hat{R}^2 + \omega^2\hat{L}^2} \frac{L - \hat{L}}{L\hat{L}} T\omega L\Delta i_d \\ &= \frac{\hat{R}^2 T + \omega T\omega\hat{L}}{\hat{R}^2 + \omega^2\hat{L}^2} \frac{\omega T}{\hat{L}}(L - \hat{L})\Delta i_d. \end{aligned} \quad (36)$$

Therefore, based on  $\Delta W_d$  and  $\Delta W_q$ , a simple feedback loop for  $\hat{R}$  and  $\hat{L}$  is developed by driving  $\Delta W_d$  and  $\Delta W_q$  into zero. Besides, in order to decouple the estimation of  $R$  and  $L$ , the parameter identification for  $R$  and  $L$  should be executed separately. In this article, the estimation of  $L$  is executed first, and, then, the estimation of  $R$  will be done.

### C. High-Frequency Motor

With the definition of the high-frequency motor,  $R$  is negligible compared with  $\omega L$  and there is

$$\hat{d}_1 \approx -\frac{\sin(\omega T)}{\omega\hat{L}}\hat{d}_2 \approx \frac{\cos(\omega T) - \hat{x}}{\omega\hat{L}}. \quad (37)$$

Substituting (29) and (37) into (28)

$$\begin{aligned} \Delta W_d &= \frac{\sin(\omega T)}{\omega\hat{L}}\tilde{x}\Delta i_d + \frac{\sin(\omega T)}{\omega\hat{L}}\tilde{y}\frac{\cos(\omega T) - x}{y}\Delta i_d \\ &\quad - \frac{\cos(\omega T) - \hat{x}}{\omega\hat{L}}\tilde{y}\frac{\sin(\omega T)}{y}\Delta i_d \end{aligned}$$

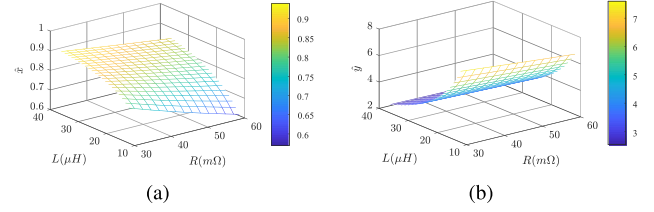


Fig. 6.  $\hat{x}$  and  $\hat{y}$  with different  $\hat{R}$  and  $\hat{L}$ . (a)  $\hat{x}$ . (b)  $\hat{y}$ .

$$\begin{aligned} &= \frac{\sin(\omega T)}{\omega\hat{L}}\tilde{x}\Delta i_d + \frac{\sin(\omega T)}{\omega\hat{L}}\frac{\tilde{y}}{y}\tilde{x}\Delta i_d \\ &= \frac{\sin(\omega T)}{\omega\hat{L}}\tilde{x}\left(1 + \frac{\tilde{y}}{y}\right)\Delta i_d = \frac{\sin(\omega T)}{\omega\hat{L}}\frac{\tilde{y}}{y}\tilde{x}\Delta i_d \end{aligned} \quad (38)$$

and

$$\begin{aligned} \Delta W_q &= \frac{\tilde{y}}{y\omega\hat{L}}(\cos(\omega T) - \hat{x})(\cos(\omega T) - x)\Delta i_d \\ &\quad + \frac{\tilde{y}}{y\omega\hat{L}}\sin^2(\omega T)\Delta i_d + \tilde{x}\frac{\cos(\omega T) - \hat{x}}{\omega\hat{L}}\Delta i_d. \end{aligned} \quad (39)$$

Clearly, it is difficult to develop a clear relationship between  $R$  and  $\hat{R}$ , or  $L$  and  $\hat{L}$ , compared with (35) and (36) in the low-frequency motor.

As shown in Fig. 6, it can be checked that  $\hat{x}$  is close to  $x$  when  $R$  and  $L$  vary by  $\pm 50\%$  compared with the change of  $\hat{y}$ . Therefore,  $\Delta W_q$  can be simplified as

$$\Delta W_q \approx \frac{\tilde{y}}{y\omega\hat{L}}(\sin^2(\omega T) + (\cos(\omega T) - x)^2)\Delta i_d. \quad (40)$$

By applying Taylor expansion,  $\tilde{y}$  can be rewritten as

$$\tilde{y} = \hat{y} - y = \frac{L - \hat{L}}{L\hat{L}}T + O(T^2) \quad (41)$$

and

$$\Delta W_q \approx \frac{(\sin^2(\omega T) + (\cos(\omega T) - x)^2)T}{y\omega L\hat{L}^2}(L - \hat{L})\Delta i_d. \quad (42)$$

Thus, a feedback loop of  $\hat{L}$  can be established. After  $\hat{L}$  converges to  $L$ , the  $\Delta W_d$  can be rewritten as

$$\Delta W_d = \frac{\sin(\omega T)}{\omega\hat{L}}\frac{\hat{y}}{y}\left(e^{-\frac{\hat{R}}{L}T} - e^{-\frac{R}{L}T}\right)\Delta i_d. \quad (43)$$

Finally, the feedback loop of  $R$  is also established.

### D. Numerical Test

Numerical test is performed to verify the effectiveness of the analysis mentioned above. The parameters of the tested low-frequency motor and high-frequency motor are shown in Tables I and II, respectively. The operating frequency is accelerated from 0 up to the rated frequency first. Then, the negative current (low-frequency motor:  $-2$  A; high-frequency motor:  $-5$  A) is injected into  $d$ -axis at 0.3 s. Based on (27),  $M_d$  and  $M_q$  have the same qualities as  $W_d$  and  $W_q$ , so  $M_d$  and  $M_q$  will be checked instead of  $W_d$  and  $W_q$ . This statement holds throughout this article.



**TABLE II**  
PARAMETERS OF THE TESTED HIGH-FREQUENCY MOTOR

Symbol	Parameter	Value
$R$	resistance	0.045 $\Omega$
$L_s$	inductance	24 $\mu\text{H}$
$U_{DC}$	DC bus voltage	48 V
$poles$	poles	2
$n_N$	the rated frequency	1.33 kHz

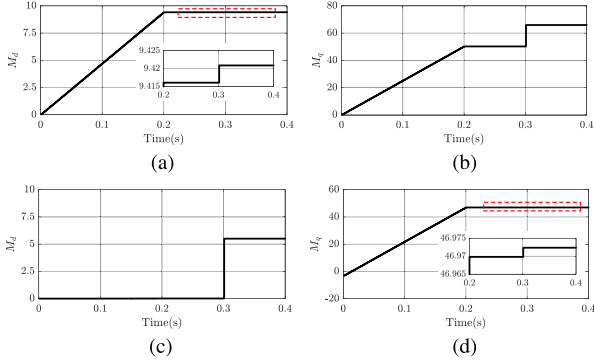


**Fig. 7.** Numerical test in the low-frequency motor:  $M_d$  and  $M_q$  with parameters adopted in Table I and negative current injected into  $d$  axis at 0.3 s. (a)  $M_d$  with 1.5  $L$  and  $R$ . (b)  $M_q$  with 1.5  $L$  and  $R$ . (c)  $M_d$  with  $L$  and 1.5 $R$ . (d)  $M_q$  with  $L$  and 1.5 $R$ .

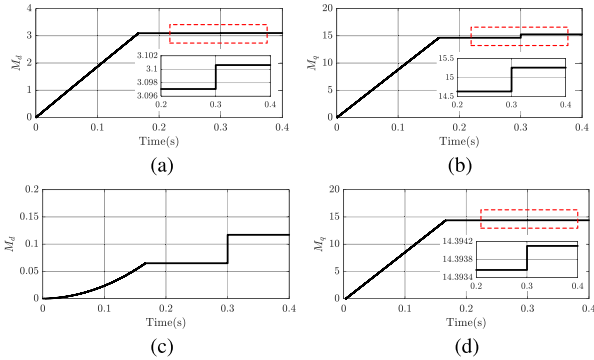


**Fig. 8.** Numerical test in the high-frequency motor:  $M_d$  and  $M_q$  with parameters adopted in Table II and negative current injected into  $d$  axis at 0.3 s. (a)  $M_d$  with 1.5  $L$  and  $R$ . (b)  $M_q$  with 1.5  $L$  and  $R$ . (c)  $M_d$  with  $L$  and 1.5 $R$ . (d)  $M_q$  with  $L$  and 1.5 $R$ .

In Fig. 7, the analysis in the low-frequency motor is tested. As shown in Fig. 7(a) and (b), with  $\hat{L} = 1.5L$  and  $\hat{R} = R$  adopted, at 0.3 s,  $M_q$  has a sharp increase while  $M_d$  basically stay unchanged. Besides, in Fig. 7(c) and (d), with  $\hat{L} = L$  and  $\hat{R} = 1.5R$  adopted, at 0.3 s,  $M_d$  has a sharp increase while  $M_q$  basically stay unchanged. It is consistent with the theoretical analysis mentioned above. The same statement can be also applied in the high-frequency motor as shown in Fig. 8.

### E. Parameter Estimator Design

In Fig. 9, the estimation structure for  $L$  and  $R$  with negative current injected into  $d$ -axis is demonstrated. It should be noted that compared to the dynamic response of the designed disturbance observer, the convergent time of  $\hat{R}$  and  $\hat{L}$  is selected to be

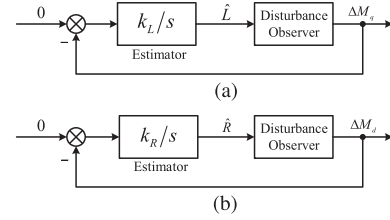


**Fig. 9.** Estimation structure for  $L$  and  $R$  with negative current injected into  $d$  axis. (a) Estimation structure for  $L$ . (b) Estimation structure for  $R$ .

long enough that its effect on the disturbance observer could be neglected. Generally, the disturbance observer will converge to steady state in several periods (less than 10). Therefore, when the convergent time of the parameter estimator for  $L$  and  $R$  is longer over 20 times than the disturbance observer, the function from  $\hat{L}$  to  $\Delta M_q$  in Fig. 9(a) and the function from  $\hat{R}$  to  $\Delta M_d$  in Fig. 9(b) can be treated as a simple proportional part. The gain  $k$  can be obtained from (35), (36), (43), and (42) and is positive, which can be adjusted by the amplitude of the injected current. When a pure integral estimator  $k_{L,R}/s$  for  $L$  and  $R$  is adopted, the open-loop and close-loop transfer functions can be expressed as

$$G_{\text{open}} = \frac{k_{L,R}k}{s} \quad G_{\text{close}} = \frac{k_{L,R}k}{s + k_{L,R}k} \quad (44)$$

where  $k_{L,R}$  is the positive gain of the integral estimator. Clearly, the stability of the parameter identification is guaranteed. The convergent rate of the parameter identification for  $R$  and  $L$  depends on the selection of the  $k_{L,R}$ . In order to ensure the convergence within the predefined time, the  $k_{L,R}$  can be chosen as follows:

$$k_{L,R} \approx \frac{\Delta}{T_p} \quad (45)$$

where  $\Delta$  is the estimated boundary of the parameter deviation of  $R$  and  $L$ .  $T_p$  is the predefined maximum convergent time. Normally, the  $T_p$  is limited and considering the convergent rate of the disturbance observer is normally less than 10  $T$ ,  $T_p$  should be larger than 200  $T$  to ensure the stability.

Besides, a dead-zone modification is implemented to improve the robustness of the parameter identification. When the  $\Delta M_q$  or  $\Delta M_d$  is within the selected dead-zone, the estimation of  $L$  or  $R$  will be bypassed.

## V. SIMULATION RESULTS

Simulation in MATLAB/Simulink is performed to validate the effectiveness of the proposed DPCC method. The parameters of the tested low-frequency and high-frequency motor are the same as in Tables I and II, respectively. The parameters of the proposed DPCC method is demonstrated in Table III.

Fig. 10 shows the performance of the proposed DPCC method with  $\hat{L} = 1.5L$  and  $\hat{R} = 1.5R$  at 133.3 Hz. In Fig. 10(a), the tracking performance of  $i_q$  is demonstrated. Before the parameter identification, with  $\hat{L} = 1.5L$  and  $\hat{R} = 1.5R$  adopted in the controller, the feed-forward voltage from the predictive current control law is larger than the desired value, therefore the

TABLE III  
PARAMETERS OF THE PROPOSED DPCC METHOD

Symbol	Parameter	Value
$f_s$	switching frequency	10 kHz
$T$	sampling period	0.0001 s
$Q$	convergent matrix	$diag(0.4, 0.4)$
$k_L$ (low frequency)	gain for $L$ estimator	0.005
$k_R$ (low frequency)	gain for $R$ estimator	4
$k_L$ (high frequency)	gain for $L$ estimator	$2 \times 10^{-5}$
$k_R$ (high frequency)	gain for $R$ estimator	0.04
$TH_L$	threshold of $L$	0.1
$TH_R$	threshold of $R$	0.03

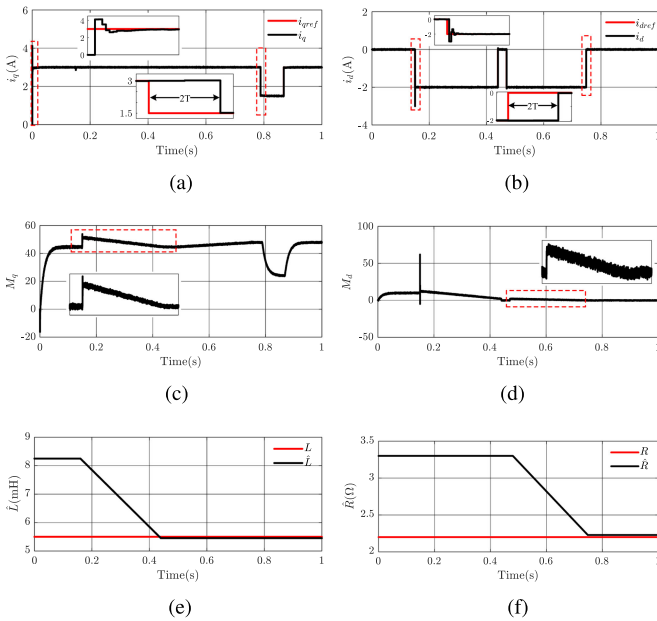


Fig. 10. Simulation results in the low-frequency motor:  $i_q$ ,  $i_d$ ,  $M_q$ ,  $M_d$ ,  $\hat{L}$  and  $\hat{R}$  with  $\hat{L} = 1.5L$  and  $\hat{R} = 1.5R$  at 133.3 Hz. (a)  $i_q$ . (b)  $i_d$ . (c)  $M_q$ . (d)  $M_d$ . (e)  $\hat{L}$ . (f)  $\hat{R}$ .

overshoot occurs. Due to the disturbance observer, the tracking error is gradually eliminated. Then, the proposed parameter identification for  $L$  and  $R$  works. In Fig. 10(b), the negative current ( $-2$  A) is injected into the  $d$ -axis. The first injection aims at the identification of  $L$ . With the current injected,  $M_q$  is increased rapidly and an integral controller for  $\hat{L}$  works to drive  $\Delta M_q$  to zero as shown in Fig. 10(c). In Fig. 10(e), the  $\hat{L}$  converge to  $L$  successfully. The second injection aims at the identification of  $R$ . With the current injection,  $M_d$  is increased rapidly in Fig. 10(d) and an integral controller for  $\hat{R}$  also works to drive  $\Delta M_d$  to zero. The  $\hat{R}$  converge to  $R$  successfully as shown in Fig. 10(f). It has to be noted that the performance before the parameters identification is consistent with [14], but as the main contribution of this article, the proposed parameters identification for  $R$  and  $L$  works and when the parameters identification is finished, the ideal deadbeat response is achieved for both  $i_q$  and  $i_d$  in Fig. 10(a) and 10(b), respectively. This is a significant improvement compared with [14].

The same statement can be applied in the high-frequency motor as shown in Fig. 11, but the  $\hat{R}$  cannot converge to  $R$

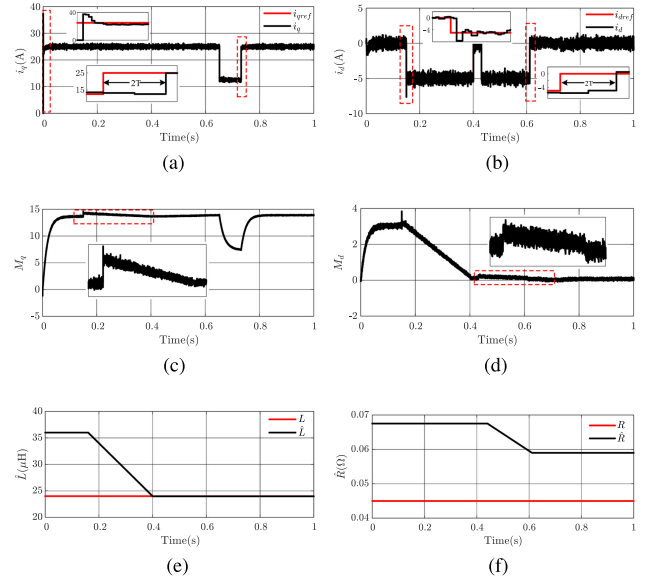


Fig. 11. Simulation results in the high-frequency motor  $i_q$ ,  $i_d$ ,  $M_q$ ,  $M_d$ ,  $\hat{L}$  and  $\hat{R}$  with  $\hat{L} = 1.5L$  and  $\hat{R} = 1.5R$  at 1.33 kHz. (a)  $i_q$ . (b)  $i_d$ . (c)  $M_q$ . (d)  $M_d$ . (e)  $\hat{L}$ . (f)  $\hat{R}$ .

in Fig. 11(f). Because the  $R$  of the tested motor is much small, the  $\Delta M_d$  caused by the injected  $i_d$  is also small and considering the nonliterary of the switching devices, it is reasonable for the estimation of  $R$  behaving as shown in Fig. 11(f). Although the estimation error of  $R$  exists, the voltage difference caused by this estimation error is adequately small compared with the command voltage. With the effectively estimated  $L$ , the ideal deadbeat response is also achieved at high operating frequency as shown in Fig. 11(a) and 11(b).

## VI. EXPERIMENTAL RESULTS

Experiments are also performed to validate the proposed DPCC method. The parameters of the tested low-frequency and high-frequency motor are also the same as Tables I and II, respectively. Additionally, all the experimental data will be sent to the host PC via the Ethernet module on the control board.

### A. Different Convergent Rating of $R$ and $L$ Identification

Fig. 12 shows the performance of the proposed DPCC with  $\hat{L} = 3$  mH and  $\hat{R} = 1$   $\Omega$  at 133.3 Hz. In Fig. 12(a), the tracking performance of  $i_q$  is demonstrated. The tested SPMSM is controlled by the torque current while the load motor is on the speed-controlled mode. Before the parameter identification, with  $\hat{L} = 3$  mH and  $\hat{R} = 1$   $\Omega$  adopted in the controller, the feed-forward voltage from the predictive current control law is smaller than the desired value, therefore, the current response is slow. With the help of the disturbance observer, the tracking error is gradually eliminated. Then, the proposed parameter identification for  $L$  and  $R$  works. In Fig. 12(b), the negative current ( $-1$  A) is injected into the  $d$ -axis. The first injection aims at the estimation of  $L$ . With the current injection,  $M_q$  is decreased rapidly and an integral controller for  $\hat{L}$  works to

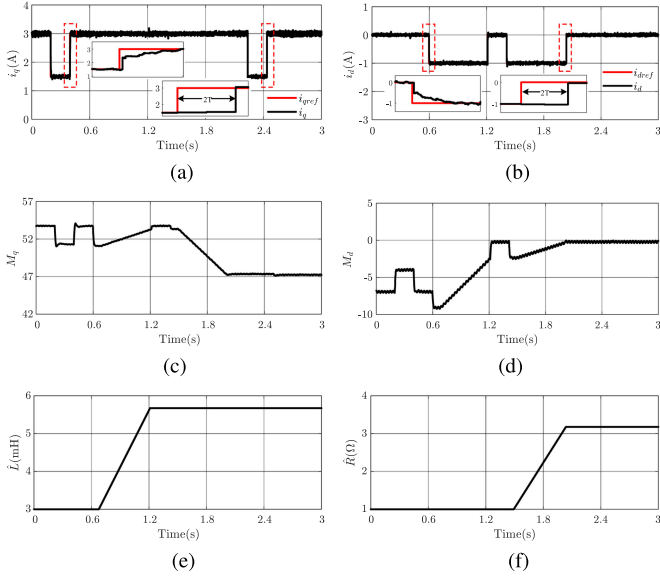


**Fig. 12.** Experimental results in the high-frequency motor:  $i_q$ ,  $i_d$ ,  $M_q$ ,  $M_d$ ,  $\hat{L}$ , and  $\hat{R}$  with  $\hat{L} = 3$  mH and  $\hat{R} = 1\Omega$  at 133.3 Hz. (a)  $i_q$ . (b)  $i_d$ . (c)  $M_q$ . (d)  $M_d$ . (e)  $\hat{L}$ . (f)  $\hat{R}$ .

drive  $\Delta M_q$  to zero as shown in Fig. 12(c). Fig. 12(e) shows the performance of the  $\hat{L}$ . The second injection aims at the estimation of  $R$ . With the current injection,  $M_d$  is decreased rapidly and an integral controller for  $\hat{R}$  also works to drive  $\Delta M_d$  to zero in Fig. 12(d). The  $\hat{R}$  converges as shown in Fig. 12(f). When the parameters identification is finished, the ideal deadbeat current control is achieved for both  $i_q$  and  $i_d$  in Fig. 12(a) and 12(b). It is worth noting that all the parameters of the tested motors are obtained by the offline measurement, which could be different from the values on the operating state. But when the estimated parameters adopted in the controller, the ideal deadbeat response is achieved, which indicates that the estimated parameters is accurate.

The same statement with  $\hat{L} = 12 \mu\text{H}$  and  $\hat{R} = 22 \text{ m}\Omega$  adopted in the controller can be applied in the high-frequency motor as shown in Fig. 13. The ideal deadbeat control is also achieved in the high-frequency motor as shown in Fig. 13(a) and 13(b).

The experimental results are well validated with the theoretical analysis and the simulation results mentioned above. The problem caused by the mismatched parameters has been essentially solved compared with [14]. Besides, the proposed parameter identification method for  $R$  and  $L$  works on both low-frequency and high-frequency motors. Clearly, this method can be implemented easily based on the disturbance observer, which is the great advantage.

As the analysis mentioned above, the convergent rate of the parameter identification for  $R$  and  $L$  depends on the selection of the  $k_{L,R}$ . So the performance of the different  $k_{L,R}$  for the estimation of  $R$  and  $L$  is investigated.

In Fig. 14, the convergent performances of  $\hat{L}$  and  $\hat{R}$  with different  $k_L$  and  $k_R$  adopted in low-frequency motor are demonstrated. Clearly, it can be observed that the larger gains are helpful for the convergence. The convergent time can be

approximately down to 26 and 22 ms in this experiment. However, when the convergent time is less than the  $200T$  (20 ms), the estimation error inevitably occurs. Therefore, the selection of  $k_L$  and  $k_R$  is limited by the convergent time and it should be larger than 20 ms. Additionally, the same statement can be also effective in the high-frequency motor at 1.33 kHz in Fig. 15.

## B. Comparison With Traditional RLS Method

A comparison between the traditional RLS method and the proposed parameter identification method is also investigated. The RLS algorithm is adopted as [18]

$$\begin{aligned}\boldsymbol{\theta}_{\text{est}}(k) &= \boldsymbol{\theta}_{\text{est}}(k-1) + \mathbf{K}(k)\boldsymbol{\varepsilon}(k) \\ \boldsymbol{\varepsilon}(k) &= \mathbf{y}(k) - \boldsymbol{\varphi}^T(k)\boldsymbol{\theta}_{\text{est}}(k-1) \\ \mathbf{K}(k) &= \mathbf{P}(k-1)\boldsymbol{\varphi}(k)[\lambda\mathbf{I} + \boldsymbol{\varphi}^T(k)\mathbf{P}(k-1)\boldsymbol{\varphi}(k)]^{-1} \\ \mathbf{p}(k) &= [\mathbf{I} - \mathbf{K}(k)\boldsymbol{\varphi}^T(k)]\mathbf{P}(k-1)/\lambda\end{aligned}\quad (46)$$

where  $\mathbf{y}$  denotes the output vector,  $\boldsymbol{\theta}_{\text{est}}$  is the estimated parameter vector,  $\boldsymbol{\varphi}$  denotes the feedback matrix,  $\lambda$  is defined as the forgetting factor, and  $\boldsymbol{\varepsilon}$  is the estimation error.

Based on the discrete-time model (7), there is

$$\begin{aligned}\mathbf{y} &= \mathbf{T}_r^{-1}\mathbf{i}_{dq} - \hat{\mathbf{G}}_2\mathbf{e}_{dq} \\ \boldsymbol{\theta} &= [x \ y]^T\boldsymbol{\theta}_{\text{est}} = [\hat{x} \ \hat{y}]^T\boldsymbol{\varphi}^T = [\mathbf{i}_{dq} \ \mathbf{v}_{dq}]\end{aligned}\quad (47)$$

where the matrix  $\hat{\mathbf{G}}_2$  is calculated by the estimated  $\hat{x}$  and  $\hat{y}$ . So the estimated parameters can be obtained as

$$\hat{R} = \frac{1 - \hat{x}}{\hat{y}}\hat{L} = -\frac{RT}{\ln \hat{x}}.\quad (48)$$

It can be observed that the output vector  $\mathbf{y}$  contains the elements concerned with the PM flux linkage  $\Psi$ , which cannot be obtained accurately. So the estimation accuracy relies on the accuracy of  $\Psi$ .

Figs. 16 and 17 demonstrate the estimation performance by the traditional RLS method with the different PM flux linkage  $\Psi$ . Considering the ideal deadbeat current response can be achieved by the proposed method, the estimated  $R$  and  $L$  via the proposed identification method can be regarded as accurate. It can be concluded that the convergent values are closely related to the selected  $\Psi$ , but the  $\Psi$  cannot be measured accurately during the rotation. Therefore, it is difficult for the traditional RLS to estimate the  $R$  and  $L$  accurately with the unknown  $\Psi$ . Additionally, the execution time between the traditional RLS method and the proposed method for DSP28335 (150 MHz) is also compared as follows. Obviously, the RLS method need more time because it contains much matrix manipulations. And the proposed method avoids them.

Method	Execution Time
Traditional RLS Method	18.9 $\mu\text{s}$
Proposed Method	0.313 $\mu\text{s}$

Another important thing should be explained. As the analysis mentioned above, the conventional RLS method cannot deal

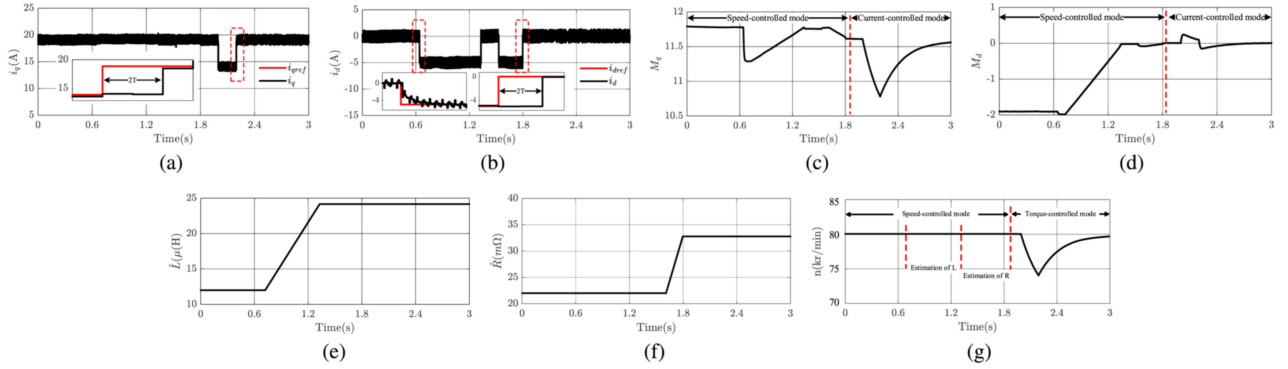


**Fig. 13.** Experimental results in the high-frequency motor:  $i_q$ ,  $i_d$ ,  $M_q$ ,  $M_d$ ,  $\hat{L}$ , and  $\hat{R}$  with  $\hat{L} = 12 \mu\text{H}$  and  $\hat{R} = 22 \text{ m}\Omega$  at 1.33 kHz. (a)  $i_q$ . (b)  $i_d$ . (c)  $M_q$ . (d)  $M_d$ . (e)  $\hat{L}$ . (f)  $\hat{R}$ . (g) speed.

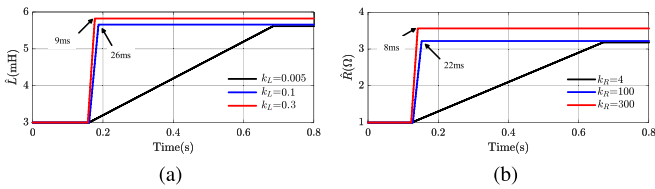


**Fig. 14.** Experimental results in the low-frequency motor: performance of the different  $k_{L,R}$  for the estimation of  $R$  and  $L$  with  $\hat{L} = 3 \text{ mH}$  and  $\hat{R} = 1 \Omega$  at 133.3 Hz. (a) Estimation of  $L$ . (b) Estimation of  $R$ .

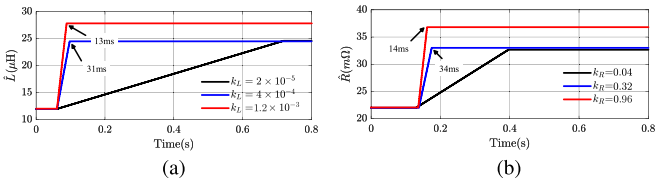


**Fig. 15.** Experimental results in the high-frequency motor: performance of the different  $k_{L,R}$  for the estimation of  $R$  and  $L$  with  $\hat{L} = 12 \mu\text{H}$  and  $\hat{R} = 22 \text{ m}\Omega$  at 1.33 kHz. (a) Estimation of  $L$ . (b) Estimation of  $R$ .

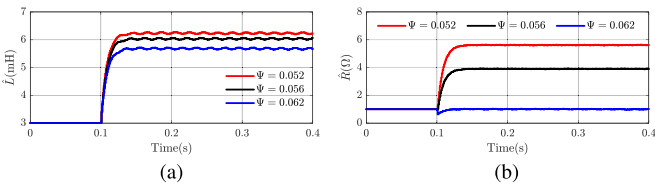


**Fig. 16.** Experimental results in the low-frequency motor: traditional RLS method for the estimation of  $R$  and  $L$  with different  $\Psi$  at 133.3 Hz ( $\hat{R} = 3.2 \Omega$  and  $\hat{L} = 5.8 \text{ mH}$  by the proposed method). (a) Estimation of  $L$ . (b) Estimation of  $R$ .

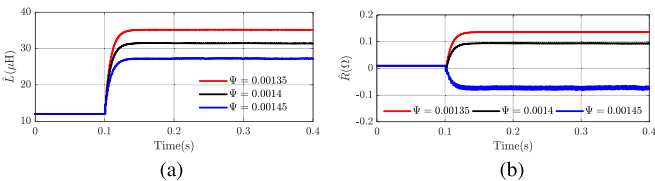


**Fig. 17.** Experimental results in the high-frequency motor: traditional RLS method for the estimation of  $R$  and  $L$  with different  $\Psi$  at 1.33 kHz ( $\hat{R} = 32 \text{ m}\Omega$  and  $\hat{L} = 24 \mu\text{H}$  by the proposed method). (a) Estimation of  $L$ . (b) Estimation of  $R$ .

with the estimation of  $R$  and  $L$  with the unknown  $\Psi$ . But several papers proposed a two-time scale method to achieve the multiparameter identification ( $R$ ,  $L$ , and  $\Psi$ ) [18], [19], [23]. However, this kind of method is not considered in this article because of the following.

- 1) The RLS method consists of much matrix manipulations and it need more time to finish them. If a two-time scale method is adopted, the execution time is not acceptable, especially for the industrial application.
- 2) The stability of the two-time scale method is not provided by theoretical analysis in these papers. Whether the estimated values have converged to the real values or not cannot be guaranteed.

## VII. CONCLUSION

This article proposed an improved DPCC method for the SPMSM with parameter identification. With the proposed DPCC method, zero steady-state current error and deadbeat dynamic current response could be achieved, even with inaccurate motor parameters. The following contributions are achieved.

- 1) The proposed parameters identification method can be implemented easily with greatly reduced computation burden compared with the traditional RLS methods.
- 2) Since the design is established based on a fully discretized model, the effectiveness will be guaranteed on both low-frequency and high-frequency motors.
- 3) With the estimated parameters adopted, the parameter mismatch problem is essentially solved and the ideal deadbeat response is achieved. This is a significant improvement compared with [14].

The effectiveness of the proposed DPCC method was validated by the simulation and experimental results on a 133.3 Hz motor and a 1.33 kHz motor with 10 kHz sampling frequency.

## REFERENCES

- [1] F. Briz, M. W. Degner, and R. D. Lorenz, "Analysis and design of current regulators using complex vectors," *IEEE Trans. Ind. Appl.*, vol. 36, no. 3, pp. 817–825, May 2000.
- [2] T. M. Rowan and R. J. Kerkman, "A new synchronous current regulator and an analysis of current-regulated PWM inverters," *IEEE Trans. Ind. Appl.*, vol. IA-22, no. 4, pp. 678–690, Jul. 1986.



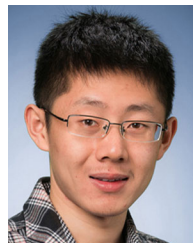
- [3] H. Kim, M. W. Degner, J. M. Guerrero, F. Briz, and R. D. Lorenz, "Discrete-time current regulator design for AC machine drives," *IEEE Trans. Ind. Appl.*, vol. 46, no. 4, pp. 1425–1435, Jul. 2010.
- [4] K. K. Huh and R. D. Lorenz, "Discrete-time domain modeling and design for AC machine current regulation," in *Proc. IEEE Ind. Appl. Annu. Meeting*, Sep. 2007, pp. 2066–2073.
- [5] M. P. Kazmierkowski and L. Malesani, "Current control techniques for three-phase voltage-source PWM converters: A survey," *IEEE Trans. Ind. Electron.*, vol. 45, no. 5, pp. 691–703, Oct. 1998.
- [6] X. Zhang, L. Zhang, and Y. Zhang, "Model predictive current control for PMSM drives with parameter robustness improvement," *IEEE Trans. Power Electron.*, vol. 34, no. 2, pp. 1645–1657, Feb. 2019.
- [7] S. Bolognani, S. Bolognani, L. Peretti, and M. Zigliotto, "Design and implementation of model predictive control for electrical motor drives," *IEEE Trans. Ind. Electron.*, vol. 56, no. 6, pp. 1925–1936, Jun. 2009.
- [8] J. Liu, C. Gong, Z. Han, and H. Yu, "IPMSM model predictive control in flux-weakening operation using an improved algorithm," *IEEE Trans. Ind. Electron.*, vol. 65, no. 12, pp. 9378–9387, Dec. 2018.
- [9] M. H. Vafaie and B. M. Dehkordi, "Approach for classifying direct PCs applied to AC motor drives," *IET Electr. Power Appl.*, vol. 13, no. 3, pp. 385–401, 2019.
- [10] S.-M. Yang and C.-H. Lee, "A deadbeat current controller for field oriented induction motor drives," *IEEE Trans. Power Electron.*, vol. 17, no. 5, pp. 772–778, Sep. 2002.
- [11] P. Wipasuramontorn, Z. Q. Zhu, and D. Howe, "Predictive current control with current-error correction for PM brushless AC drives," *IEEE Trans. Ind. Appl.*, vol. 42, no. 4, pp. 1071–1079, Jul. 2006.
- [12] J. S. Lee, C. Choi, J. Seok, and R. D. Lorenz, "Deadbeat-direct torque and flux control of interior permanent magnet synchronous machines with discrete time stator current and stator flux linkage observer," *IEEE Trans. Ind. Appl.*, vol. 47, no. 4, pp. 1749–1758, Jul. 2011.
- [13] Y. Jiang, W. Xu, C. Mu, and Y. Liu, "Improved deadbeat predictive current control combined sliding mode strategy for PMSM drive system," *IEEE Trans. Veh. Technol.*, vol. 67, no. 1, pp. 251–263, Jan. 2018.
- [14] X. Zhang, B. Hou, and Y. Mei, "Deadbeat predictive current control of permanent-magnet synchronous motors with stator current and disturbance observer," *IEEE Trans. Power Electron.*, vol. 32, no. 5, pp. 3818–3834, May 2017.
- [15] L. Rovere, A. Formentini, and P. Zanchetta, "FPGA implementation of a novel oversampling deadbeat controller for PMSM drives," *IEEE Trans. Ind. Electron.*, vol. 66, no. 5, pp. 3731–3741, May 2019.
- [16] X. Ding, S. Wang, M. Zou, and M. Liu, "Predictive current control for permanent magnet synchronous motor based on MRAS parameter identification," in *Proc. IEEE Int. Power Electron. Appl. Conf. Expo.*, Nov. 2018, pp. 1–5.
- [17] N. Li, M. Yang, and X. Dianguo, "An adaptive robust predictive current control for PMSM with online inductance identification," *Int. Rev. Elect. Eng.*, vol. 7, pp. 3845–3856, Mar. 2012.
- [18] S. J. Underwood and I. Husain, "Online parameter estimation and adaptive control of permanent-magnet synchronous machines," *IEEE Trans. Ind. Electron.*, vol. 57, no. 7, pp. 2435–2443, Jul. 2010.
- [19] D. Q. Dang, M. S. Rifaq, H. H. Choi, and J. Jung, "Online parameter estimation technique for adaptive control applications of interior PM synchronous motor drives," *IEEE Trans. Ind. Electron.*, vol. 63, no. 3, pp. 1438–1449, Mar. 2016.
- [20] P. Niazi and H. A. Toliyat, "Online parameter estimation of permanent-magnet assisted synchronous reluctance motor," *IEEE Trans. Ind. Appl.*, vol. 43, no. 2, pp. 609–615, Mar. 2007.
- [21] T. Boileau, N. Leboeuf, B. Nahid-Mobarakeh, and F. Meibody-Tabar, "Online identification of PMSM parameters: Parameter identifiability and estimator comparative study," *IEEE Trans. Ind. Appl.*, vol. 47, no. 4, pp. 1944–1957, Jul. 2011.
- [22] Y. Yao, Y. Huang, and F. Peng, "Position sensorless drive of high speed permanent magnet synchronous motor," in *Proc. IEEE Energy Convers. Congr. Expo.*, Sep. 2018, pp. 1733–1740.
- [23] M. S. Rifaq, F. Mwasilu, J. Kim, H. H. Choi, and J. Jung, "Online parameter identification for model-based sensorless control of interior permanent magnet synchronous machine," *IEEE Trans. Power Electron.*, vol. 32, no. 6, pp. 4631–4643, Jun. 2017.



drive system with *LCL* output filter.



all-electric ships, more-electric aircraft, and wind power generation systems.



interests include design, modeling, and control of electromechanical systems.



interests include design, modeling, and control of electromechanical systems.



control of PMSM servo system.

**Yu Yao** received the B.S. degree in electrical engineering in 2016 from Southeast University, Nanjing, China, where he is currently working toward the Doctor of Engineering degree in electric machines and control with the School of Electrical Engineering.

His main research interests include the design of the power inverter, the current regulator design, the position sensorless drive for the high-speed surface-mounted permanent magnet synchronous machines (SPMSM), and the

**Yunkai Huang** received the M.Sc. and Ph.D. degrees in electrical engineering from Southeast University, Nanjing, China, in 2001 and 2007, respectively.

He is currently a Professor with the School of Electrical Engineering, Southeast University and teaching "Electrical Machinery" and "Digital Signal Processing". His research interests include design and control of PM machine and high speed machine, applications in domestic appliances, electric vehicles, railway traction,

all-electric ships, more-electric aircraft, and wind power generation systems.

**Fei Peng** received the B.S. and M.S. degrees in electrical engineering from Southeast University, Nanjing, China, in 2010 and 2012, respectively. He received the Ph.D. degree in electrical and computer engineering from McMaster University, Hamilton, ON, Canada, in 2016.

After that he was a Postdoctoral Fellow with the McMaster Institute for Automotive Research and Technology, McMaster University. In December 2016, he joined the School of Electrical Engineering, Southeast University as an Assistant Professor. His research interests include optimal design and control of power converters, modeling, and digital control of motor drives.

**Jianning Dong** received the B.S. and Ph.D. degrees in electrical engineering from Southeast University, Nanjing, China, in 2010 and 2015, respectively.

Since 2016, he has been an Assistant Professor with the Delft University of Technology (TU Delft), Delft, 682 Netherlands and is teaching "Electromechanics". Before joining TU Delft, he was a Postdoctoral Researcher with McMaster Automotive Resource Centre, McMaster University, Hamilton, ON, Canada. His main research

interests include design, modeling, and control of electromechanical systems.

**Hanqi Zhang** received the B.S. degree in electrical engineering from the Nanjing University of Aeronautics and Astronautics, Nanjing, China, in 2018. She is currently working toward the M.E. degree in electric machines and control with the School of Electrical Engineering, Southeast University, Nanjing, China.

Her main research interests include the current regulator design, disturbance observer, nonlinear modeling of permanent magnet synchronous machine (PMSM), and the position

control of PMSM servo system.